

# Bioactive Antifouling Surfaces by Visible-Light-Triggered Polymerization

Andriy R. Kuzmyn, Ai T. Nguyen, Han Zuilhof,\* and Jacob Baggerman\*

Hierarchical bioactive surfaces are created by visible-light-induced surface-initiated living radical polymerization employing tris[2-phenylpyridinato-C2,N] iridium(III) as a photocatalyst. The hierarchical antifouling diblock copolymer structures consist of *N*-(2-hydroxypropyl)-methacrylamide (first block) and carboxybetaine methacrylate (second block). The living nature of the polymerization is shown by a linear increase in layer thickness (as measured by atomic force microscopy) and reinitiation of the polymerization to create a patterned second block of polymer. The chemical structure of the brushes is confirmed by X-ray photoelectron spectroscopy and attenuated total reflection Fourier transform infrared spectroscopy measurements. The block copolymer brushes demonstrate excellent antifouling properties when exposed to single-protein solutions or to bovine serum. The second carboxybetaine block of the hierarchical antifouling structures can effectively be biofunctionalized with an anti-fibrinogen antibody. The coated surfaces show a high affinity and specificity to fibrinogen, while preventing nonspecific adsorption from other proteins in bovine serum.

or other active biological elements of interest.<sup>[2]</sup> Nevertheless, many bioactive surfaces exposed to complex biological media have difficulties curbing the non-specific adoption of proteins.<sup>[3]</sup> Therefore, practical application of such bioactive layers requires the incorporation of antifouling layers.<sup>[4]</sup>

Different strategies are employed for creating such antifouling coatings, including functional self-assembled monolayers (SAMs),<sup>[5]</sup> polymer layers by “grafting-to” methods,<sup>[6,7]</sup> and polymer brushes by “grafting-from” methods.<sup>[8–13]</sup> For example, oligo(ethyleneglycol)-terminated alkyl SAMs are able to resist or decrease fouling from single-protein solutions.<sup>[14]</sup> Also poly(ethyleneglycol) (PEG) polymer-coated surfaces obtained by grafting-to methods show significant resistance to nonspecific protein adsorption.<sup>[15]</sup> Nevertheless, nei-

ther of these approaches is able to fully prevent fouling from complex biological matrices such as blood plasma or serum.<sup>[16,17]</sup> In contrast, polymer brushes created by grafting-from methods have demonstrated remarkable resistance to biofouling from complex biological matrices, especially those based on zwitterionic polymers,<sup>[18,19]</sup> such as polycarboxybetaines based on the corresponding methacrylate/amide (CBMA),<sup>[12,20]</sup> polysulfobetaines from their methacrylate/amide precursor (SBMA),<sup>[9,21,22]</sup> but also formally uncharged polymer brushes derived from *N*-(2-hydroxypropyl) methacrylamide (HPMA).<sup>[10,23]</sup>

Surface-initiated atom transfer radical polymerization (SI-ATRP) is the most frequently used approach for creating antifouling polymer brush coatings.<sup>[10,13,24]</sup> However, SI-ATRP is a thermal reaction that requires a rigorous control over oxygen-free reaction conditions, which makes the reaction difficult to scale up and only provides uniform coatings. In response, new and easy-to-use approaches toward versatile polymer brush coatings were developed,<sup>[25,26]</sup> such as activator regenerated by electron transfer (ARGET)<sup>[12,27]</sup> and initiators for continuous activator regeneration (ICAR).<sup>[28]</sup> In addition, light-induced polymerizations have been developed, so as to allow spatial and temporal control over the surface coating.<sup>[29]</sup> For example, surface-initiated photoinduced single-electron transfer living radical polymerization reactions (SET-LRP)<sup>[23]</sup> and surface-initiated photoiniferter-mediated polymerization (SI-PIMP)<sup>[8,20]</sup> have been used to create antifouling polymer brushes. However, those techniques utilize UV light that is not suitable for all types of monomers, as it may trigger uncontrolled photopolymerizations. Recently, a new technique was introduced for surface-initiated visible-light-triggered living

## 1. Introduction


Bioactive surfaces have an indispensable role in a variety of biomedical applications such as biosensing, tissue engineering, and bioimplants.<sup>[1]</sup> Those surfaces optimally display immobilized bioactive molecules that can interact with cells, proteins

A. R. Kuzmyn, Dr. A. T. Nguyen, Dr. J. Baggerman  
Aquamarijn Micro Filtration BV  
IJsselkade 7, 7201 HB Zutphen, The Netherlands  
E-mail: jacob.baggerman@wur.nl

Prof. H. Zuilhof, Dr. J. Baggerman  
Laboratory of Organic Chemistry  
Wageningen University  
Stippeneng 4, 6708 WE Wageningen, The Netherlands  
E-mail: han.zuilhof@wur.nl

Prof. H. Zuilhof  
School of Pharmaceutical Sciences and Technology  
Tianjin University  
92 Weijin Road, Tianjin 300072, P. R. China

Prof. H. Zuilhof  
Department of Chemical and Materials Engineering  
King Abdulaziz University  
21589 Jeddah, Saudi Arabia

 The ORCID identification number(s) for the author(s) of this article can be found under <https://doi.org/10.1002/admi.201900351>.

© 2019 Wageningen University. Published by WILEY-VCH Verlag GmbH & Co. KGaA, Weinheim. This is an open access article under the terms of the Creative Commons Attribution-NonCommercial-NoDerivs License, which permits use and distribution in any medium, provided the original work is properly cited, the use is non-commercial and no modifications or adaptations are made.

DOI: 10.1002/admi.201900351

radical polymerization (LT-LRP) mediated by transition metal-based photoredox chemistry, e.g., by iridium complexes.<sup>[30–33]</sup> This method requires only a small amount of catalyst and allows to create, in a highly controlled manner, complex patterns of polymer brushes using visible light.<sup>[32,34]</sup>

A good bioactive antifouling layer balances two objectives, namely, maximizing immobilization of bioreceptors and minimizing the nonspecific adsorption of proteins.<sup>[4,35]</sup> However, a significant amount of immobilized bioreceptors itself increases the nonspecific adsorption of proteins, due to fouling nature of bioreceptors on their own, as well as due to the changes in antifouling brush structure.<sup>[36,37]</sup> In contrast, a low amount of immobilized bioreceptors might decrease the biosensing capabilities of the bioactive surfaces, but better maintains the antifouling properties of the polymer brushes. The balance between these two factors determines the performance of antifouling bioactive surfaces, i.e., robust antifouling behavior and efficient capture of analytes.

The effective biofunctionalization of polymer brushes without impairing antifouling properties still poses a challenge. The two main methods used for post-polymerization biofunctionalization of antifouling polymer brushes are chain-end modification<sup>[24,38,39]</sup> and side-chain modification.<sup>[10,40]</sup> The latter method can be achieved using three different approaches via homopolymers with reactive side chains,<sup>[18]</sup> copolymers with both reactive and unreactive side chains,<sup>[36]</sup> or third, diblock copolymer brushes with only the upper block being functionalized.<sup>[39]</sup> The immobilization of the bioactive elements on the chain end of polymer brushes allows to largely preserve the structure of the brush and its antifouling properties. However, the quantity of immobilized bioactive molecules via chain-end modification is significantly lower than that via side-chain functionalization. The side-chain modification approach is typically based on activating functional groups of the side chains of (co)polymer brush. This approach allows reactive groups to react with biomolecules to immobilize a large quantity of biomolecules along the chain, while still maintaining significant antifouling. Two recent examples led us to our current work. First, the combination of a sulfobetaine with a clickable but still zwitterionic sulfobetaine, which allows fully 3D loading of biomolecules.<sup>[21]</sup> Second, a random copolymer brush of *N*-(2-hydroxypropyl) methacrylamide and carboxybetaine methacrylamide (CBMAA), in which the latter could be bioconjugated via the use of activated ester reactions.<sup>[37]</sup> While both aspects highlight important facets in particular high loading of bioactive moieties, the first approach starts to display loss of antifouling properties upon high degrees of loading, while the second impairs the structure of the brush causing changes in the hydrodynamic properties of the polymer chains, crosslinking of lateral chains, and steric hindrance. Diblock copolymer brushes with only the upper block modification might constitute a compromise approach that allows to immobilize a significant number of biomolecules where they can most readily interact with the biomarkers of interest (i.e., near the outside of the brush), and simultaneously nearly fully preserves the lower block of the antifouling polymer brush structure and consequently the antifouling properties of whole system.<sup>[41,42]</sup>

Herein, we introduce a robust and facile method for the formation of temporally and spatially tuned antifouling bioactive

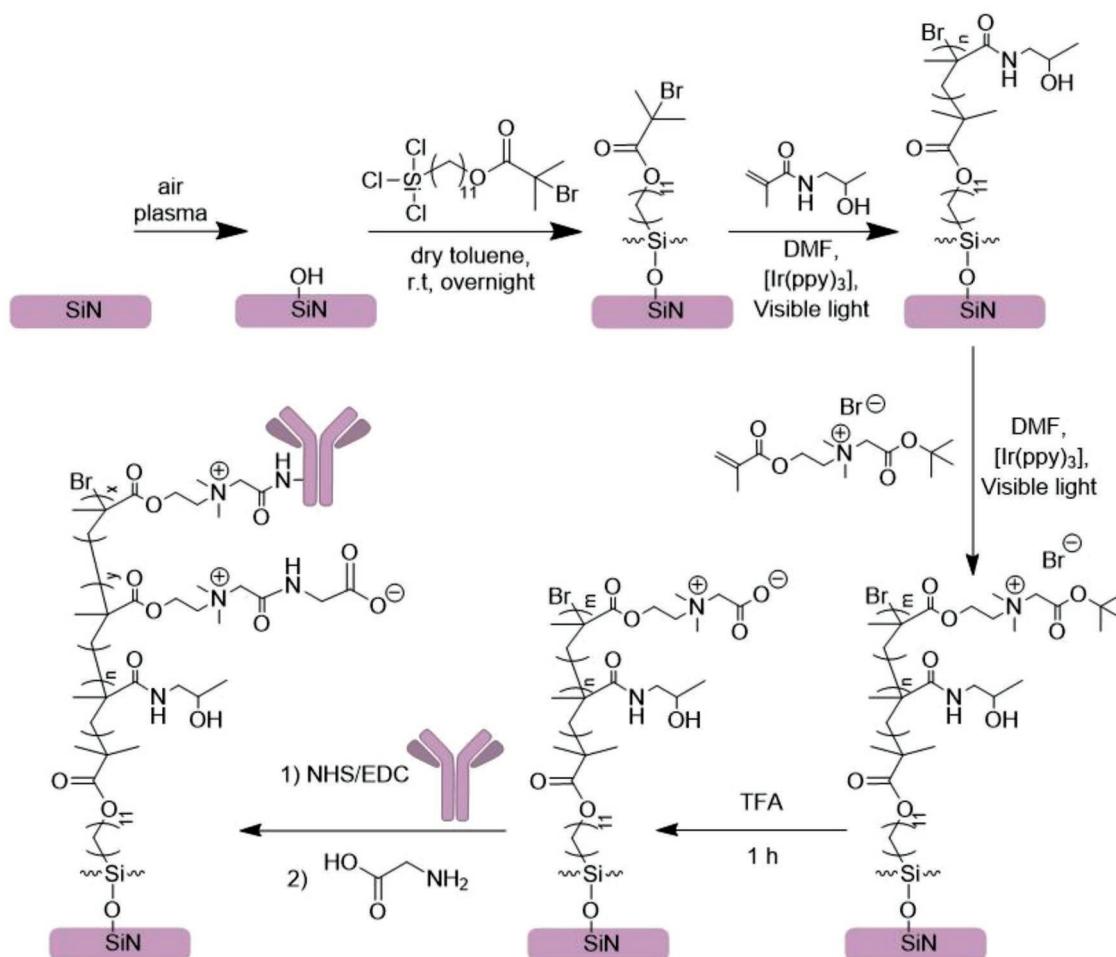
polymer brushes using LT-LRP. With this method we synthesized for the first time biofunctional antifouling diblock copolymer brushes based on *N*-(2-hydroxypropyl) methacrylamide at the bottom of the brush, and carboxybetaine methacrylate (CBMA) at the top. The resulting brushes were characterized extensively by X-ray photoelectron spectroscopy (XPS), atomic force microscopy (AFM), attenuated total reflection Fourier-transform infrared spectroscopy (ATR-FTIR), and scanning Auger microscopy. The bottom poly(HPMA) block was chosen because it seems to yield the best antifouling properties of the routinely studied brushes,<sup>[10,40,43]</sup> while the poly(CBMA) brushes display high antifouling properties even after significant functionalization.<sup>[18,40]</sup> We outline that the Ir(ppy)<sub>3</sub>-mediated light-triggered surface-initiated living radical polymerization allows for well-controlled polymerization conditions and for further reinitiation from poly(HPMA) brush. Moreover, we show that this technique yields spatial control over the brush formation and biofunctionalization.<sup>[32]</sup> The antifouling character, as studied by fluorescence microscopy, is verified in single protein solutions and also in complex biological media. Finally, we demonstrate selective capture by antibody functionalized poly(CBMA) in complex media, which indicates the application potential of these block copolymer brushes.

## 2. Results and Discussions

The method employed to create hierarchical bioactive antifouling diblock copolymer brushes consists of four consecutive steps including LT-LRP (**Scheme 1**). First, from an initiator-coated silicon nitride surface poly(HPMA) brushes are grown via LT-LRP. Subsequently, a chain extension was performed from the poly(HPMA)-coated surfaces with a protected carboxybetaine derivative. The carboxybetaine monomer was chosen for the second block because of the exceptional antifouling properties of the CBMA-based polymer brushes and for the well-explored synthetic pathways of biofunctionalization of those brushes.<sup>[18]</sup> A *tert*-butyl ester-protected carboxybetaine methacrylate-based poly(CBMA-*t*Bu) was utilized, as direct polymerization of carboxybetaine monomers did not succeed (see below).<sup>[44]</sup> Third, deprotection of the protected carboxyl groups in the poly(CBMA-*t*Bu) polymer yielded the carboxybetaine polymer. Finally, bioactive moieties were coupled to the CBMA block via NHS/EDC activation of the carboxyl groups.

### 2.1. Visible Light-Triggered Polymerization of Poly(HPMA) Brushes

The poly(HPMA) brushes of different thickness were grown from self-assembled monolayers of 11-(trichlorosilyl)undecyl-2-bromo-2-methylpropanoate by LT-LRP. The selected trichlorosilane self-assembled monolayers have been previously reported as suitable for anchoring of polymer brushes.<sup>[23,45,46]</sup> The successful grafting of the initiator monolayer was confirmed by XPS. The XPS narrow-scan spectrum of the C1s region (Figure S1a, Supporting Information) shows three



**Scheme 1.** Schematic depiction of the method to create hierarchical bioactive surfaces. Poly(CBMA)-poly(HPMA)-diblock brushes are grown from an initiator SAM on silicon nitride via LT-LRP, and subsequently biofunctionalized via activation of the carboxyl groups of poly(CBMA) polymer block.

peaks. The peak at 285.0 eV is attributed to the carbon atoms in the alkyl backbone of the initiator, and the peaks at 286.7 and 289.3 eV are assigned to the carbon atoms adjacent to the ester [C–O] and bromide [C–Br], and the carbon from the carbonyl group, respectively. The observed ratio between [C–C/H]: [C–O]: [C–Br]: [C=O] peaks is 12.1: 1.0: 1.1: 0.8, which corresponds to the theoretically expected ratio of 12: 1: 1: 1. Also, the experimentally obtained spectrum corresponds well to a simulated XPS spectrum (Figure S2, Supporting Information) based on the core orbital energy levels calculated by density functional theory (DFT).<sup>[47,48]</sup> In addition, peaks of the bromine end-group were found at 71 eV in the XPS Br3d narrow-scan spectrum (Figure S1b, Supporting Information), further confirming the presence of the initiator on the surface.

Poly(HPMA) brushes with different thicknesses were grown from the initiator-coated surfaces by LT-LRP utilizing Ir(ppy)<sub>3</sub> as a photocatalyst. The kinetics of the polymer brush growth—from 0 to ≈ 80 nm—were followed by measuring by AFM the dry thickness of the polymer layer as function of the reaction time. The AFM topography images of brush-coated surfaces revealed homogeneous layers with an average roughness of *R*<sub>q</sub> of 1.5 ± 0.3 nm (Figure S3a, Supporting Information). The thickness of the brush increased linearly in time, which

confirms the controlled nature of the polymerization (Figure 1a and Table S1, Supporting Information). The polymerization proceeded faster using an light-emitting diode (LED, 380 nm) compared to a halogen lamp (white light, see emission spectrum, Figure S4, Supporting Information), with an average rate of polymerization of 13.2 ± 0.6 and 9.6 ± 0.6 nm h<sup>-1</sup>, respectively. This could be caused by both the difference in intensity between these light sources and the higher absorption coefficient of Ir(ppy)<sub>3</sub> at 380 nm, compared to that at visible-light wavelengths (see spectrum of light absorption, Figure S5, Supporting Information). The dependence of the polymerization rate on the light intensity was previously demonstrated by Hawker and coworkers.<sup>[31]</sup> A higher light intensity leads to an increased amount of excited photocatalyst and therefore more activation of the polymerization initiator occurs. The possibility of using a conventional broad-emission light source, such as a halogen lamp, confirms the ease of use and robustness of this approach for creating antifouling layers.

The chemical structure of the synthesized poly(HPMA) brushes was confirmed by ATR-FTIR (Figure 2a). The FTIR spectrum of poly(HPMA) brushes with a thickness of 20 nm shows the typical broad stretching bands of hydroxyl (O–H) and amide (N–H) bonds around 3300 cm<sup>-1</sup>. The C=O stretch

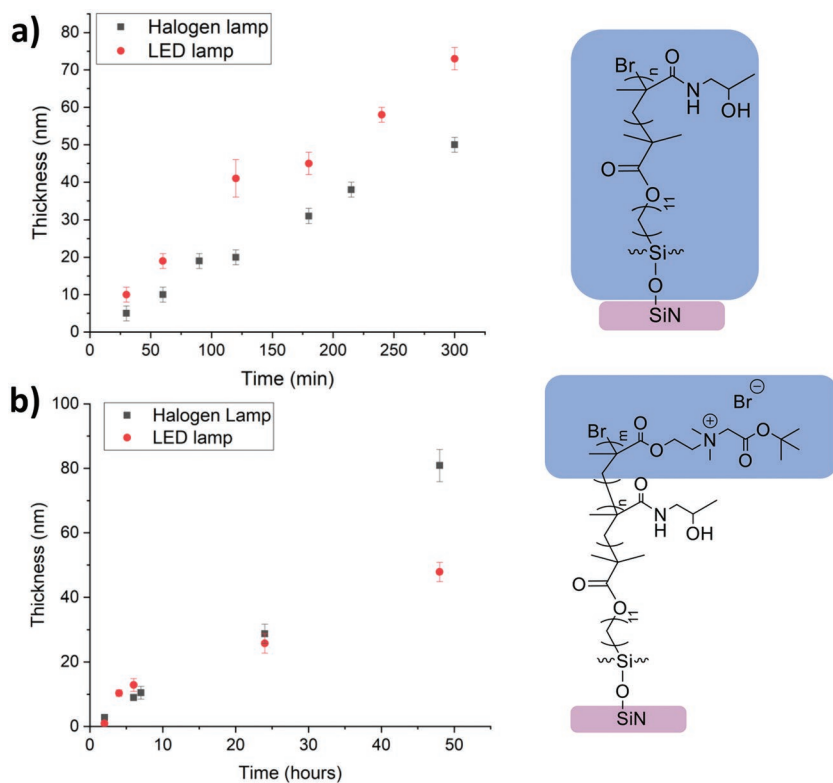


**Figure 1.** Dry thickness of polymer brushes as function of the polymerization time, as determined by AFM a) for poly(HPMA) and b) for poly(CBMA-tBu) grown from the poly(HPMA) macroinitiator with thickness of 20 nm.

(amide I) and the coupled N–H deformation and C–N stretch (amide II) bands of the secondary amide group are visible at 1650 and 1530  $\text{cm}^{-1}$ , respectively. The weak absorption at 1730  $\text{cm}^{-1}$  corresponds to C=O stretching of the ester groups present in the initiator layer. These results are in good agreement with the expected chemical structure of poly(HPMA) on the surfaces.

The chemical structure was further confirmed by XPS. The wide-scan XPS spectrum shows – after the various washing steps – no residual iridium on the poly(HPMA)-coated surfaces (Figure S6, Supporting Information). The narrow-scan XPS C1s spectrum (Figure 2c), measured on poly(HPMA)-coated surface with a thickness of 20 nm, displays a broad peak at 285 eV with a shoulder between 286–287 eV, attributed to overlapping signals, and a smaller peak at 288 eV attributed to the carbonyl atom. The spectrum was deconvoluted by fitting it with four peaks centered at 285.0 eV assigned to C–H and C–C bound atoms, at 285.9 eV from the C–N atoms, at 286.6 eV from the C–O atoms, and at 287.9 eV from the C=O atoms. The ratio between [C–C/H]: [C–N]: [C–O]: [N–C=O] peaks is 3.8: 1.1: 1.1: 1.0, which is in excellent agreement with the theoretically expected composition of the poly(HPMA) structure (4: 1: 1: 1). Moreover, the C1s spectrum correlates well with the simulated C1s XPS spectrum obtained by DFT calculations (See Figure S7 in the Supporting Information).<sup>[47,48]</sup> The combination of AFM, XPS, and IR data thus clearly confirm the presence of poly(HPMA) brushes on the initiator-coated surface.

## 2.2. Introduction of Second Block of Poly(CBMA-tBu) on Poly(HPMA)

The living nature of the LT-LRP polymerization should allow to grow a second polymer block from the poly(HPMA) brush macroinitiator. Initial attempts to grow polymer brushes of CBMA on poly(HPMA) by LT-LRP with  $\text{Ir}(\text{ppy})_3$  in mixtures of water, ethanol, methanol, and DMF resulted in self-polymerization of the solution. Polymerization of CBMA in DMF or other nonprotic polar solvents was not possible due to solubility issues of the monomer. Thus, a carboxyl-protected monomer, CBMA-tBu, was used for the synthesis of the second block. The AFM topography measurement confirmed an overall homogeneous layer without irregularities and pinholes and featuring a roughness of  $R_q = 1.2 \pm 0.3$  nm (Figure S4b, Supporting Information). The kinetics of growth of poly(CBMA-tBu) brush was again linear, thereby confirming that controlled nature of this polymerization step (Figure 1b and Table S2, Supporting Information). The rate of polymerization of the CBMA-tBu monomer (halogen lamp  $1.5 \pm 0.2$  nm  $\text{h}^{-1}$  and LED lamp  $1.1 \pm 0.3$  nm  $\text{h}^{-1}$ ) is lower due to the charged nature of this monomer, which causes repulsion of the approaching monomer by the growing charged polymer

brushes. This has been observed for this monomer before, showing also a low polymerization rate with conventional ATRP.<sup>[49]</sup> In addition, the temporary stop of the first polymerization might also lead to some termination reactions that would overall lead to a slower polymerization after reinitiation, although this effect has been shown to be small for neutral monomers.<sup>[31,32]</sup> The chemical structure of the CBMA-tBu copolymer was confirmed by ATR-FTIR (Figure 2a) and XPS. In the ATR-FTIR spectrum of poly(CBMA-tBu)-poly(HPMA)-coated surfaces a strong ester-based C=O stretching peak appears at 1733  $\text{cm}^{-1}$ , i.e., significantly different from the amide-based C=O peak at 1650  $\text{cm}^{-1}$  observed for the poly(HPMA) block. The XPS N1s narrow scan (Figure 2b) shows an additional peak at 402.6 eV, which indicates the presence of positively charged nitrogen [ $\text{N}^+$ ] in the chemical structure of the layer. The peak at 399.5 eV in those spectra corresponds to the neutral nitrogen [N–H] present in the poly(HPMA) layer below the second block. The relatively high intensity of the [N–H] peak, even with a 10 nm second poly(CBMA-tBu) block, is probably due to a relative low density of the latter. The charged nature of CBMA-tBu and bulky nature of tBu group in the monomer can cause the polymer chains to repel each other, which likely results in a lower density of the second block. Moreover, the XPS C1s narrow scan spectrum (Figure 2c) shows the appearance of a peak at 289.5 eV attributed to ester carbon atoms [O–C=O], and an increase in intensity of the peaks at 286.0 eV [C–N], and 286.7 eV [C–O]. The overall data demonstrate the successful growth of poly(CBMA-tBu) brushes from

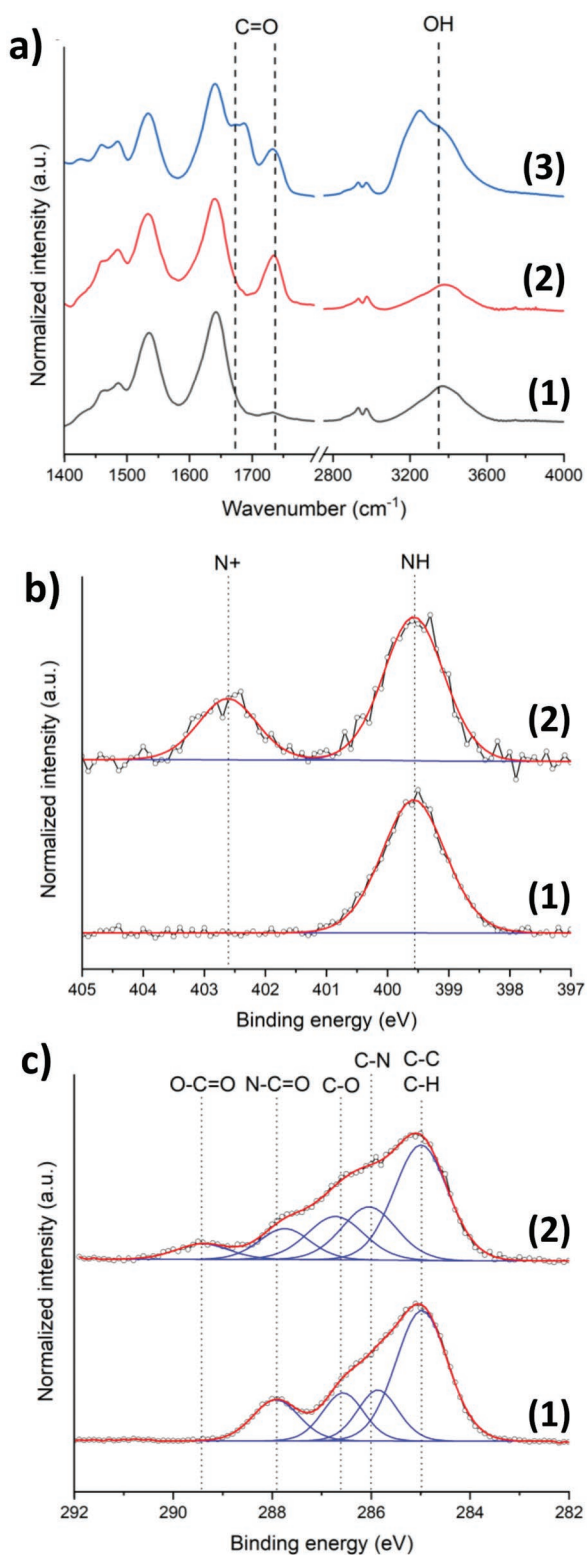


**Figure 2.** a) ATR-FTIR spectra of 1) poly(HPMA) brushes with a thickness of 20 nm, 2) poly(HPMA)-poly(CBMA-tBu) copolymer with a total thickness of 30 nm, and 3) poly(HPMA)-poly(CBMA) copolymer thickness of 30 nm. Narrow-range XPS spectra of the b) N1s and c) C1s regions for 1) poly(HPMA) brushes with thickness of 20 nm, and 2) poly(HPMA)-poly(CBMA-tBu) copolymer with thickness of 30 nm.

poly(HPMA) macroinitiator yielding poly(CBMA-tBu) layer as a second block of the copolymer.

In order to generate a zwitterionic CBMA polymer top block, the *tert*-butyl ester moieties of the poly(CBMA-tBu)-poly(HPMA) diblock polymer brush structures were deprotected by exposure to undiluted trifluoroacetic acid at room temperature for 1 h. The ATR-FTIR spectrum of the deprotected poly(CBMA)-block-poly(HPMA) shows the appearance of a new peak at  $1670\text{ cm}^{-1}$  corresponding to the C=O stretching vibrations of the carboxylic acid groups. Also, an increase in the intensity of the hydroxyl stretching at  $3200\text{ cm}^{-1}$  was observed. These changes indicate the occurrence of the carboxylic acid groups in the copolymer (Figure 2a). Moreover, the XPS wide-scan spectra (Figures S8 and S9, Supporting Information) show a decrease of the carbon signals relative to the oxygen and nitrogen signals, which is in line with the loss of carbon due to the hydrolysis of the *tert*-butyl ester. In addition, no traces of iridium could be detected after polymerization and deprotection of the CBMA-tBu.

### 2.3. Patterning of Poly(CBMA-tBu) Brushes

An advantage of the LT-LRP approach is that it enables the formation of complex 3D-structured copolymer brush layers by using a mask and tuning the thickness of the different blocks. This was demonstrated by the growth of CBMA-tBu on poly(HPMA) with a patterning mask. From various observations, it became clear that the poly(CBMA-tBu) only grew in irradiated regions, whereas no growth was observed in regions without illumination. First, the resulting patterns could be easily observed with an optical microscope (Figure 3a), because the SiN surface changes its color in a regular fashion with a change of the thickness of the polymer brush layer on top. The dark pinkish stripes correspond to the thinner poly(HPMA) layer, the green to the poly(HPMA)-poly(CBMA-tBu) layer and the scratch (yellowish) in the middle of Figure 3a reveals the bare silicon nitride underneath, which was used as reference for the thickness evaluation. Second, the 3D structure of corresponding layers was also confirmed by AFM studies of a uniformly coated poly(HPMA) layer onto which a pattern of locally grown poly(CBMA-tBu) was attached. Figure 3b shows a uniform poly(HPMA) layer thickness of 20 nm and a poly(HPMA)-poly(CBMA-tBu) layer thickness of 50 nm. The thickness of 20 nm for the poly(HPMA) layer corresponds to the thickness before patterning, which demonstrates that the second block only grew in the illuminated areas. Third, the selective growth of the poly(CBMA-tBu) top block was further confirmed by Auger intensity mapping of the nitrogen signal at 382 eV (Figure 3d). The different amount of neutral nitrogen [N–H] in patterned areas and nonpatterned areas is shown by different intensities of red color.

This patterned growth thus also opened up the possibility of local biofunctionalization of the designed patterned layer, via the local immobilization of BSA-FITC on the surface. After deprotection (see above), the CBMA surfaces were biofunctionalized with BSA-FITC utilizing NHS/EDC active ester chemistry. Only fluorescence was observed in the CBMA-patterned areas, indicating that BSA-FITC was only present in these areas

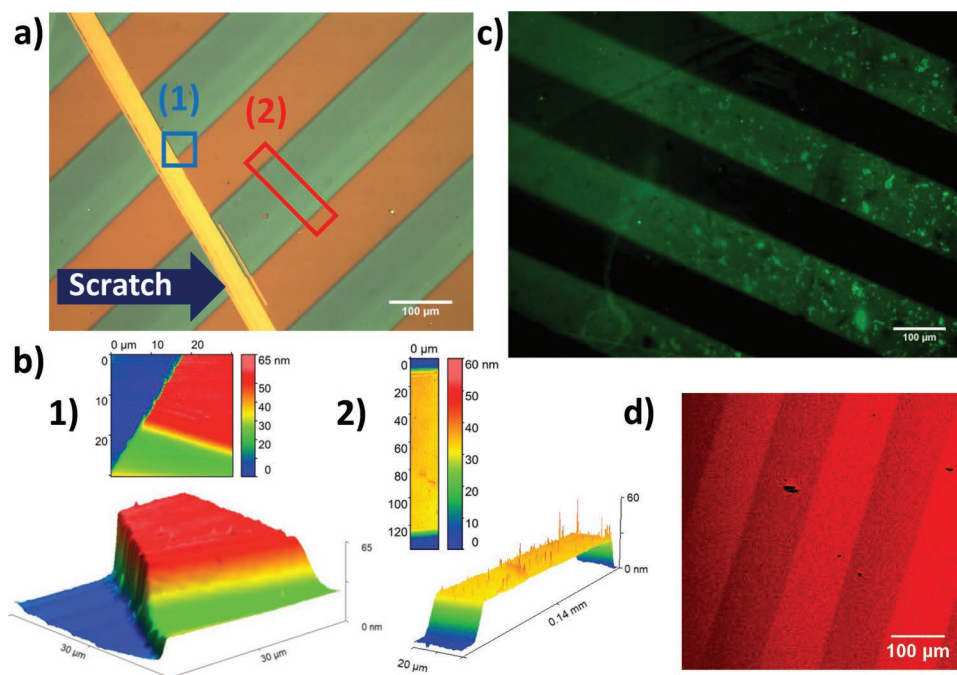


**Figure 3.** a) Optical microscope image of line-patterned 30 nm thick poly(CBMA-tBu) layer on a uniformly coated 20 nm thick poly(HPMA) layer, with a scratch (orange bar) that was used as reference for the thickness measurement. b) AFM topography of Sections 1 and 2 in (a). c) Fluorescence microscope image of a deprotected patterned poly(CBMA-tBu) layer with immobilized BSA-FITC. d) Intensity mapping of the nitrogen Auger signal at 382 eV.

(Figure 3c). This approach enables the local biofunctionalization of antifouling surfaces, while the antifouling property in the nonfunctionalized areas is unaffected.

#### 2.4. Biospecific Capture with Poly(CBMA)-Poly(HPMA)-Coated Surfaces

To demonstrate the applicability of the poly(CBMA)-poly(HPMA)-coated surfaces for biosensing applications, anti-fibrinogen (AntiFbg) antibodies were immobilized on the surfaces. Fibrinogen (Fbg) was chosen as an analyte, since it also shows significant nonspecific adsorption on nonmodified surfaces and has been frequently used as a model protein for fouling determination. AntiFbg has strong affinity to the  $\alpha$ -chain of human fibrinogen, allowing an efficient capture of fibrinogen. The immobilization of AntiFbg was achieved by activating the carboxylate groups along the CBMA chains using NHS/EDC chemistry and subsequently binding the antibody via active ester coupling. The design of bioactive surfaces requires to have not only high affinity to the analyte but also an excellent resistance to fouling from complex biological media. Therefore, poly(CBMA)-poly(HPMA)-coated surfaces were used with thicknesses of 20 nm for the HPMA and 10 nm for the CBMA block. The thicknesses of these blocks were chosen to balance between antifouling performance of the bottom layer—for which typically >15 nm brushes are required—and loading of bioactive elements and antifouling performance of the top layer.<sup>[50]</sup> A thicker second block allows for a higher loading of antibody but—since antibodies themselves are not antifouling, but rather: fouling—at the same time might reduce the fouling performance.

The coated surfaces were challenged by contacting them with fluorescent single-protein solutions of BSA-FITC, Fbg-Alexa647, and Str-FITC, respectively, and by a 10% biotinylated bovine serum (BS) solution in PBS for 15 min; this time is typically sufficient to assess the adsorption of proteins onto stable polymer brushes.<sup>[10]</sup> The fouling by biotinylated BS was detected by subsequent exposure to Str-FITC solution, which binds to the biotin residues of any fouling serum proteins present on the surface.<sup>[43]</sup> The fluorescence intensity of exposed bare SiN surfaces is high, due to the high nonspecific adsorption of proteins from corresponding solutions (Figure 4a and Table S3, Supporting Information). The introduction of poly(HPMA) on the surface of SiN drastically lowers the intensity of fluorescence after exposure to biofouling solutions. This confirms that poly(HPMA) brushes synthesized by the LT-LRP technique preserve its original highly effective antifouling properties, as previously reported for poly(HPMA) brushes synthesized with ATRP and SET-LRP methods.<sup>[10,23]</sup> The diblock copolymer structure of poly(HPMA) and poly(CBMA) also showed similarly high antifouling properties to the three single-protein solutions as well as to the biotinylated bovine serum solution. Both poly(HPMA) and poly(CBMA) are strongly hydrated polymers leading to their excellent antifouling properties.<sup>[10,43,51]</sup>

The bioactive antifouling surface was created by biofunctionalizing the second block of poly(HPMA)-poly(CBMA) with AntiFbg antibodies. The resulting surface was exposed as well to the different single-protein solutions and to the biotinylated bovine serum solution. The poly(HPMA)-poly(CBMA)-AntiFbg showed excellent resistance to the nonspecific adsorption of Str-FITC, BSA-FITC and biotinylated serum proteins. In addition, it demonstrated the effective and specific capture of Fbg-Alexa647 from single protein solution (Figure 4a) compared

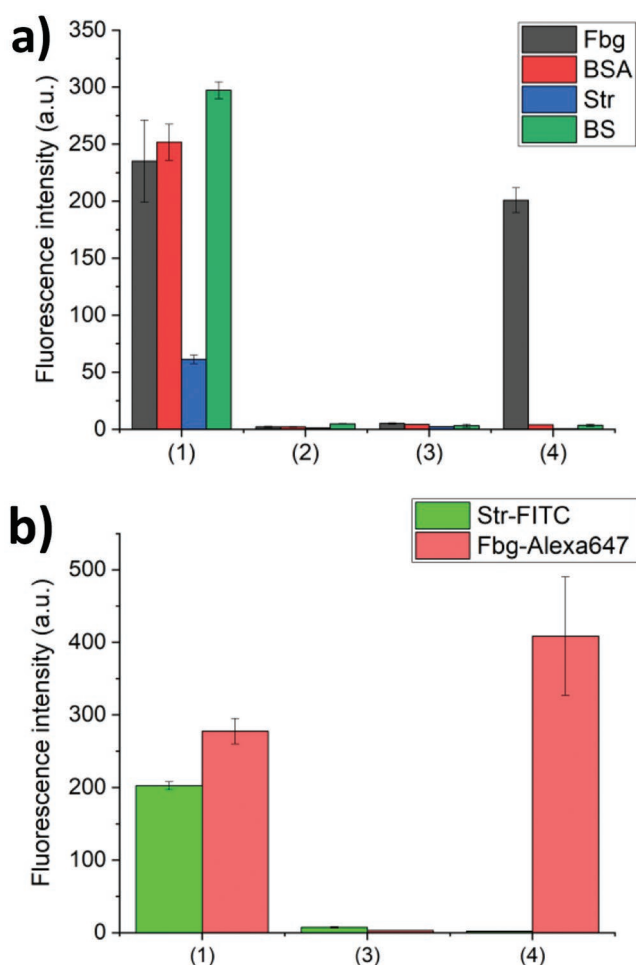


**Figure 4.** a) Fluorescence intensities of Fbg-Alexa647 (0.1 mg mL<sup>-1</sup>), BSA-FITC (0.1 mg mL<sup>-1</sup>), Str-FITC (0.1 mg mL<sup>-1</sup>), and Str-FITC labeled 10% diluted biotinylated bovine serum (BS) on 1) bare SiN 2), poly(HPMA), 3) poly(CBMA)-poly(HPMA), and 4) AntiFbg-poly(CBMA)-poly(HPMA). b) Fluorescence intensities of Fbg-Alexa647 (0.1 mg mL<sup>-1</sup>) in 10% diluted biotinylated bovine serum. The Str-FITC was used for labeling proteins from bovine serum labeled with fluorescent signal attributed to nonspecific adsorption of proteins from bovine serum.

with the nonfunctionalized poly(CBMA)-poly(HPMA) (two-tailed *t*-test probability  $P < 0.0001$ ,  $P = 2 \times 10^{-8}$ ). Moreover, we compared the capture of Fbg-Alexa647 by the diblock structure AntiFbg-poly(CBMA)-poly(HPMA) with an AntiFbg-functionalized dense poly(carboxybetaine acrylamide) brush (poly(CBMAA)). The poly(CBMAA) brush, with a thickness of 17 nm, was synthesized by SI-ATRP according to a previously published procedure.<sup>[10]</sup> The AntiFbg-poly(CBMA)-poly(HPMA) coated surfaces showed a 49% higher ( $P < 0.01$ ) fluorescence intensity compared with AntiFbg-poly(CBMAA) (Figure S10 and Table S5, Supporting Information). This indicates that the diblock strategy allows for a higher antibody loading for capture of Fbg-Alexa647. The higher loading is most likely due to the lower density of the second block in the poly(HPMA)-poly(CBMA) coating, as indicated by the visibility of the HPMA amide nitrogen atom in the XPS spectrum (see above). Previous studies of bioactive antifouling hierarchical

polymer brush structures also indicated that a lower grafting density for the second layer may allow for a higher loading of antibody.<sup>[52]</sup>

We have further challenged the created AntiFbg-poly(CBMA)-poly(HPMA)-coated surfaces, for specific capture not only from single-protein solution but also from complex biological media, by exposing the surface to BS containing Fbg-Alexa647 (0.1 mg mL<sup>-1</sup>). Also, here the fouling from BS was detected by fluorescence from Str-FITC that labeled the adsorbed biotinylated BS proteins. The specific capture was detected by fluorescence from Fbg-Alexa647. On bare silicon nitride fluorescence was observed from both BS labeled with Str-FITC and Fbg-Alexa647 (Figure 4b and Table S4, Supporting Information). The bare silicon nitride has lower fluorescence intensities of protein adsorption from BS compared with the intensities observed for BS without Fbg-Alexa647 added. This is most likely due to the presence of Fbg-Alexa647 that also adsorbs on the surface and replaces some adsorbed BS proteins (Vroman effect). While on the poly(CBMA)-poly(HPMA)-coated surfaces nearly no fluorescence was observed from both the BS and Fbg (Figure 4b). However, on the AntiFbg functionalized block copolymer only fluorescence from the Fbg-Alexa647 was observed. The significant fluorescent signal of Fbg-Alexa647 as analyte and no signal from fouling of proteins attributed to BS on the surface that were exposed to BS containing Fbg-Alexa647 (0.1 mg mL<sup>-1</sup>). The fluorescence signal from Fbg-Alexa647 on the AntiFbg-poly(CBMA)-poly(HPMA)-coated surfaces is significantly higher ( $P < 0.0001$ ) in case of capture from BS compared to that from single-protein solutions. A possible reason for this might be interaction of Fbg with other proteins present in the serum, in particular thrombin. This could cause dimerization of Fbg into fibrin dimers or oligomers, which can also be captured by AntiFbg on the surfaces.<sup>[53]</sup> Nevertheless, these results pave the way for the creation of biosensors that recognize analytes selectively in different complex biological media.

### 3. Conclusion

We designed a new approach to create bioactive polymer brush-coated surfaces using light-triggered living radical polymerization. We demonstrated the potential of this approach to obtain patterned biospecific polymer brushes on top of an independently patternable nonfouling base layer. As an example in case, *N*-(2-hydroxypropyl) methacrylamide (HPMA, 1st block) and carboxybetaine methacrylate (CBMA, 2nd block) were grown successively from initiator-coated surfaces via LT-LRP with Ir(ppy)<sub>3</sub>. The designed diblock copolymers showed excellent antifouling properties in single-protein solutions of bovine serum albumin, streptavidin and fibrinogen, and also in diluted bovine serum medium. Furthermore, conjugation of anti-human fibrinogen antibody on the poly(HPMA)-poly(CBMA)-coated surfaces demonstrated the high selectivity of the bioreceptor to fibrinogen in complex biological medium without impairment of the proteins resistance. We thus envision that the strategy presented herein can be efficiently applied in highly sensitive biosensing devices, along several lines currently ongoing in our labs.

## 4. Experimental Section

**Materials:** All chemical reagents were used without further purification, unless otherwise specified. Tris[2-phenylpyridinato-C<sub>2</sub>,N]iridium(III) (Ir(ppy)<sub>3</sub>), *N,N*-dimethylformamide (DMF), 2-(dimethylamino)ethyl methacrylate, *tert*-butyl bromoacetate, *N*-hydroxysuccinimide (NHS), *N*-(3-dimethylaminopropyl)-*N*-ethylcarbodiimide hydrochloride (EDC), and albumin fluorescein isothiocyanate conjugate from bovine serum (BSA-FITC) were purchased from Sigma-Aldrich, and *N*-(2-hydroxypropyl) methacrylamide from Polysciences, Inc. Fibrinogen from human plasma, Alexa Fluor 647 conjugate (Fbg-Alexa647), and mouse anti-fibrinogen monoclonal antibody (AntiFbg) were acquired from Thermo Fisher Scientific. Streptavidin-fluorescein isothiocyanate conjugate (Str-FITC) was purchased from BD Biosciences. 11-(Trichlorosilyl)undecyl-2-bromo-2-methylpropanoate was purchased from Gelest, Inc. Silicon substrates coated with 50 nm of LPCVD silicon nitride were acquired from Siltronix. Deionized water was produced with Milli-Q Integral 3 system Millipore, Molsheim, France (Milli-Q water). Bovine serum was obtained and biotinylated as previously described.<sup>[43]</sup>

**2-*tert*-Butoxy-*N*-(2-(methacryloyloxy)ethyl)-*N,N*-dimethyl-2-oxoethanaminium (CBMA-*t*Bu) monomer synthesis.** The synthesis was performed as previously reported.<sup>[49]</sup> 2-(Dimethylamino)ethyl methacrylate (5.00 g, 31.8 mmol) and *tert*-butyl bromoacetate (8.68 g, 34.3 mmol) were reacted in acetonitrile (20 mL) for 24 h at 50 °C under Ar protection. Following the addition of ethyl ether (250 mL) to the reaction mixture, the product precipitated, and the obtained white crystals were isolated and dried under vacuum. The resulting CBMA-*t*Bu monomer was immediately stored under argon protection at -20 °C.

<sup>1</sup>H NMR (D<sub>2</sub>O)  $\delta$  (ppm): 1.40 (s, 9H, -OC(CH<sub>3</sub>)<sub>3</sub>), 1.83 (s, 3H, CH<sub>2</sub>=C(CH<sub>3</sub>)COO-), 3.26 (s, 6H, -CH<sub>2</sub>N(CH<sub>3</sub>)<sub>2</sub>CH<sub>2</sub>COO-), 3.94 (t, 2H, *J* = 3 Hz, -COOCH<sub>2</sub>CH<sub>2</sub>N(CH<sub>3</sub>)<sub>2</sub>CH<sub>2</sub>-), 4.23 (s, 2H, CH<sub>2</sub>N(CH<sub>3</sub>)<sub>2</sub>CH<sub>2</sub>COO-), 4.56 (t, 2H, *J* = 3 Hz, CH<sub>2</sub>=C(CH<sub>3</sub>)COOCH<sub>2</sub>CH<sub>2</sub>N(CH<sub>3</sub>)<sub>2</sub>), 5.70 and 6.06 (s, 2H, CH<sub>2</sub>=C(CH<sub>3</sub>)COO-). Yield: 90% (see Figure S11 in the Supporting Information for the NMR spectrum).

**Light Source:** A halogen lamp (see Figure S4 in the Supporting Information for the emission spectrum) and an LED with maximum intensity at 380 nm (Intelligent LED Solutions product number: ILS-XO05-S380-0058-SC211-W2) were used. The light intensity of the halogen lamp was measured to be 3.5  $\mu$ W cm<sup>-2</sup>; the LED current was set at 700 mA, corresponding to a total radiometric power of 2.9 W, according to manufacturer specifications.

**Formation of Initiator-Functionalized Self-Assembled Monolayers:** The substrates were rinsed with, acetone, absolute ethanol (EtOH), and Milli-Q water and blown dry under a gentle stream of Ar. Subsequently, the surfaces were exposed to an air plasma in a plasma cleaner (Diener electronic GmbH, Germany) for 5 min. The freshly activated surfaces were immediately immersed in a freshly prepared solution of 11-(trichlorosilyl)undecyl-2-bromo-2-methylpropanoate (1 mg mL<sup>-1</sup>) in dry toluene at RT for 16 h. The substrates were subsequently rinsed with toluene, acetone, EtOH, and Milli-Q water and blow dried with Ar.

**Synthesis of Visible-Light-Triggered Poly(HPMA) Brush:** HPMA monomer (536 mg, 3.74 mmol) was dissolved in DMF (2 mL). The obtained solution was deoxygenated by bubbling Ar through for 30 min under stirring and kept in the dark by wrapping the flask in aluminum foil. Subsequently, Ir(ppy)<sub>3</sub> (3 mg, 4  $\mu$ mol) was added to the solution under Ar protection. The polymerization solution was stirred for 15 min and transferred by syringe to individual deoxygenated crimped vials containing the initiator-coated SiN wafer substrates, which were closed immediately afterward. Immediately after this, the polymerization was conducted by irradiating the vials with visible light from a halogen or LED light source for different periods of time. In these experiments, the light source was placed 3–4 cm from the substrates and an airflow was used to cool the vials. The polymerization was stopped by turning off the light. The samples were removed from the solution and subsequently rinsed with DMF, acetone, absolute ethanol, and water, and blown dry under a gentle stream of Ar (see for a picture of the set-up Figure S12, Supporting Information).

**Formation of Poly(CBMA-*t*Bu) Brushes Grown on Poly(HPMA)-Coated Surfaces:** CBMA-*t*Bu monomer (285 mg, 0.95 mmol) was dissolved in DMF (2 mL). The obtained solution was deoxygenated by bubbling through with Ar for 30 min under stirring and in the dark by wrapping the flask in aluminum foil. Afterward, Ir(ppy)<sub>3</sub> (3 mg, 4  $\mu$ mol) was added to the solution under argon flow. The polymerization solution was stirred for 15 min and transferred via syringe to individual deoxygenated crimped vials containing poly(HPMA) coated SiN substrates, which were closed immediately afterward. Subsequently, the polymerization was conducted by irradiating the vials with visible light from a halogen or LED light source for different periods of time. The light source was placed 3–4 cm from the substrates and an airflow was used to cool the vials. The polymerization was stopped by turning off the light. The samples were removed from the solution and subsequently rinsed with DMF, acetone, absolute ethanol, and water, and dried by blowing with Ar.

**Micro-Patterned Poly(CBMA-*t*Bu) on Poly(HPMA)-Coated Surfaces:** A specifically designed micro-patterned mask (see Figure S13, Supporting Information) was placed on top of a poly(HPMA)-coated silicon nitride surface and placed in a vial. The micro-patterned brushes of poly(CBMA-*t*Bu) were grown on the of poly(HPMA) brush surface using the same procedure of chain extension of poly(HPMA) as described above.

**Deprotection of Poly(CBMA-*t*Bu) Moieties:** The poly(CBMA-*t*Bu)-poly(HPMA)-coated surfaces were immersed in trifluoroacetic acid for 1 h at RT to remove the *t*Bu protective groups, and generate a poly(CBMA) block. Afterward, the samples were washed with Milli-Q water and ethanol and dried by blowing with Ar.

**Biofunctionalization of Poly(CBMA)-Poly(HPMA):** The poly(CBMA)-poly(HPMA)-coated surfaces were incubated in freshly filtered Milli-Q water for 15 min at RT, followed by incubating in a mixture of NHS (5 mL, 0.1 M) and EDC (5 mL, 0.5 M) in 10  $\times$  10<sup>-3</sup> M NaCl for 30 min. Afterward, the activated surface was washed with Milli-Q water, and incubated for 30 min in a protein (BSA-FITC or AntiFbg, 0.1 mg mL<sup>-1</sup>) solution in phosphate-buffered saline (PBS; pH 7.4). The residual of noncovalently bound proteins was removed by rinsing with PBS and Milli-Q water. The surface was deactivated with glycine blocking solution (pH 6.0, 1 M) for 30 min, and afterward rinsed with Milli-Q water.

**Fluorescence Microscopy:** Fluorescence images of the patterned bioactive layers were taken with a widefield fluorescent microscope (Zeiss Axioskop 2+). A Leica TCS SP8 confocal laser scanning microscope (CLMS) (Leica Microsystems, Mannheim, Germany) was used to measure protein fouling and specific interactions of the coated surfaces. A Leica HyDTM hybrid detector was used in photon counting mode to measure the intensity of the fluorescence signal. A 10  $\times$  objective was used and the samples were set in focus by maximizing the reflected light intensity from the laser. Fluorescence images were obtained by accumulating 10 consecutive images. Images were analyzed with the Leica LAS X Life Science software.

**Protein Adsorption and Selective Capture:** The protein fouling and selective capture ability of the coated surfaces in complex biological media were investigated by incubating surfaces in BSA-FITC (0.1 mg mL<sup>-1</sup>), Fbg-Alexa647 (0.1 mg mL<sup>-1</sup>), Str-FITC (0.1 mg mL<sup>-1</sup>), 10% diluted biotinylated bovine serum, and in 10% diluted biotinylated bovine serum containing Fbg-Alexa647 (0.1 mg mL<sup>-1</sup>) for 15 min at RT. The surfaces exposed to biotinylated bovine serum were then copiously washed with PBS (10 mL, pH 7.4), followed by exposure to Str-FITC (0.1 mg mL<sup>-1</sup>) for 15 min at RT. Afterward the samples were rinsed with PBS (10 mL, pH 7.4) and Milli-Q water (10 mL), and subsequently dried by blowing with Ar. Further, the samples were mounted on glass slides and the intensity of fluorescence of adsorbed proteins was measured.

**X-Ray Photoelectron Spectroscopy:** XPS measurements were performed using a JPS-9200 photoelectron spectrometer (JEOL Ltd., Japan). All the samples were analyzed using a focused monochromated Al K X-ray source (spot size of 300  $\mu$ m) radiation at 12 kV and 20 mA with an analyzer energy pass of 10 eV. XPS wide-scan and narrow-scan spectra were obtained under UHV conditions (base pressure 3  $\times$  10<sup>-7</sup> Torr). All narrow-range spectra were corrected with a linear background before



fitting. The spectra were fitted with symmetrical Gaussian/Lorentzian (GL(30)) line shapes using CasaXPS. All spectra were referenced to the C1s peak attributed to C–C and C–H atoms at 285.0 eV.

**Attenuated Total Reflection Fourier-Transform Infrared Spectroscopy:** IR spectra were recorded on a Bruker Tensor 27 FT-IR spectrometer (Massachusetts, United States) with an Auto Seagull Pro IR attachment and Ge hemispherical ATR crystal attachment. The spectrum of an unmodified plasma cleaned sample was measured as a background and was subtracted from the spectra of modified samples. In addition, a linear baseline correction was applied. Spectra were acquired with 256 scans at a resolution of 4 cm<sup>-1</sup>. The starting angle was set at 68°, and with the p-polarization angle was 90° (horizontally polarized).

**Atomic Force Microscopy:** AFM surface topography images were acquired by an Asylum Research MFP-3D SA AFM (Oxford Instruments, United Kingdom). A sharp knife was used to scratch the surfaces. The scratched surfaces were sonicated in a mixture of Milli-Q water and absolute EtOH (1:1) to remove the residuals from scratching. The surfaces were subsequently dried with Ar, and the scratched surfaces were directly measured by AFM. The height differences between scratched and intact surface in AFM topography images were used to determine the thickness of polymer layers. Gwyddion software was used to process and analyze the AFM topography images.<sup>[54]</sup>

**Scanning Auger Microscopy:** Scanning Auger measurements were performed at room temperature with a scanning Auger electron microscope (JEOL Ltd., Japan, JAMP-9500F field emission scanning Auger microprobe) system. Elemental mapping was analyzed by scanning Auger microscopy. Elemental images were acquired with a primary beam of 10 keV and 8 nm probe diameter was used. The take-off angle of the instrument was 0°.

**Electronic Core Level Calculations:** All calculations were done with the GAUSSIAN 16 program.<sup>[55]</sup> The geometries of the different systems were optimized at the B3LYP/6-311G(d,p) level of theory. Natural bond orbital (NBO) analysis was employed to obtain the core orbital energies.<sup>[56]</sup>

## Supporting Information

Supporting Information is available from the Wiley Online Library or from the author.

## Acknowledgements

This project has received funding from the European Union's Horizon 2020 research and innovation program under the Marie Skłodowska-Curie grant agreement No 720325, FoodSmartphone. The authors thank Esther van Andel, Sidharam Pujari, Jan Willem Borst, Barend van Lagen, Ileana Micu, and Cees van Rijn for insightful discussions and technical assistance.

## Conflict of Interest

The authors declare no conflict of interest.

## Keywords

biosensing, controlled living polymerization, nonfouling coatings, zwitterionic polymer brushes

Received: February 25, 2019

Revised: April 4, 2019

Published online:

[1] D. F. Williams, *Biomaterials* **2009**, *30*, 5897.

[2] E. Wischerhoff, N. Badi, J.-F. Lutz, A. Laschewsky, *Soft Matter* **2010**, *6*, 705.

[3] A. T. Nguyen, R. van Doorn, J. Baggerman, J. M. J. Paulusse, M. M. Klerks, H. Zuilhof, C. J. M. van Rijn, *Adv. Mater. Interfaces* **2015**, *2*, 1400292.

- [4] Q. Yu, Y. Zhang, H. Wang, J. Brash, H. Chen, *Acta Biomater.* **2011**, *7*, 1550.
- [5] R. G. Chapman, E. Ostuni, S. Takayama, R. E. Holmlin, L. Yan, G. M. Whitesides, *J. Am. Chem. Soc.* **2000**, *122*, 8303.
- [6] S. I. Jeon, J. D. Andrade, *J. Colloid Interface Sci.* **1991**, *142*, 159.
- [7] K. C. Andree, A. M. C. Barradas, A. T. Nguyen, A. Mentink, I. Stojanovic, J. Baggerman, J. van Dalum, C. J. M. van Rijn, L. W. M. M. Terstappen, *ACS Appl. Mater. Interfaces* **2016**, *8*, 14349.
- [8] T. Matsuda, S. Ohya, *Langmuir* **2005**, *21*, 9660.
- [9] A. T. Nguyen, J. Baggerman, J. M. J. Paulusse, C. J. M. van Rijn, H. Zuilhof, *Langmuir* **2011**, *27*, 2587.
- [10] C. Rodriguez-Emmenegger, E. Brynda, T. Riedel, M. Houska, V. Šubr, A. B. Alles, E. Hasan, J. E. Gautrot, W. T. S. Huck, *Macromol. Rapid Commun.* **2011**, *32*, 952.
- [11] M. Zamfir, C. Rodriguez-Emmenegger, S. Bauer, L. Barner, A. Rosenhahn, C. Barner-Kowollik, *J. Mater. Chem. B* **2013**, *1*, 6027.
- [12] D. Hong, H.-C. Hung, K. Wu, X. Lin, F. Sun, P. Zhang, S. Liu, K. E. Cook, S. Jiang, *ACS Appl. Mater. Interfaces* **2017**, *9*, 9255.
- [13] J. O. Zoppe, N. C. Ataman, P. Mocny, J. Wang, J. Moraes, H.-A. Klok, *Chem. Rev.* **2017**, *117*, 1105.
- [14] M. Rosso, A. T. Nguyen, E. de Jong, J. Baggerman, J. M. J. Paulusse, M. Giesbers, R. G. Fokkink, W. Norde, K. Schroën, C. J. M. van Rijn, H. Zuilhof, *ACS Appl. Mater. Interfaces* **2011**, *3*, 697.
- [15] L. Chen, R. Zeng, L. Xiang, Z. Luo, Y. Wang, *Anal. Methods* **2012**, *4*, 2852.
- [16] A. de los Santos Pereira, C. Rodriguez-Emmenegger, F. Surman, T. Riedel, A. B. Alles, E. Brynda, *RSC Adv.* **2014**, *4*, 2318.
- [17] C. Rodriguez Emmenegger, E. Brynda, T. Riedel, Z. Sedlakova, M. Houska, A. B. Alles, *Langmuir* **2009**, *25*, 6328.
- [18] S. Jiang, Z. Cao, *Adv. Mater.* **2010**, *22*, 920.
- [19] J. B. Schlenoff, *Langmuir* **2014**, *30*, 9625.
- [20] J. E. Krause, N. D. Brault, Y. Li, H. Xue, Y. Zhou, S. Jiang, *Macromolecules* **2011**, *44*, 9213.
- [21] S. C. Lange, E. van Andel, M. M. J. Smulders, H. Zuilhof, *Langmuir* **2016**, *32*, 10199.
- [22] Z. Wang, E. van Andel, S. P. Pujari, H. Feng, J. A. Dijkman, M. M. J. Smulders, H. Zuilhof, *J. Mater. Chem. B* **2017**, *5*, 6728.
- [23] M. Vorobii, A. de los Santos Pereira, O. Pop-Georgievski, N. Y. Kostina, C. Rodriguez-Emmenegger, V. Percec, *Polym. Chem.* **2015**, *6*, 4210.
- [24] A. R. Kuzmyn, A. de los Santos Pereira, O. Pop-Georgievski, M. Bruns, E. Brynda, C. Rodriguez-Emmenegger, *Polym. Chem.* **2014**, *5*, 4124.
- [25] K. Matyjaszewski, *Adv. Mater.* **2018**, *30*, 1706441.
- [26] X. Pan, M. Fantin, F. Yuan, K. Matyjaszewski, *Chem. Soc. Rev.* **2018**, *47*, 5457.
- [27] Y. Song, G. Ye, Y. Lu, J. Chen, J. Wang, K. Matyjaszewski, *ACS Macro Lett.* **2016**, *5*, 382.
- [28] D. Konkolewicz, A. J. D. Magenau, S. E. Averick, A. Simakova, H. He, K. Matyjaszewski, *Macromolecules* **2012**, *45*, 4461.
- [29] X. Pan, M. A. Tasdelen, J. Laun, T. Junkers, Y. Yagci, K. Matyjaszewski, *Prog. Polym. Sci.* **2016**, *62*, 73.
- [30] J. Lalevée, M.-A. Tehfe, F. Dumur, D. Gigmes, N. Blanchard, F. Morlet-Savary, J. P. Fouassier, *ACS Macro Lett.* **2012**, *1*, 286.
- [31] J. E. Poelma, B. P. Fors, G. F. Meyers, J. W. Kramer, C. J. Hawker, *Angew. Chem., Int. Ed.* **2013**, *52*, 6844.
- [32] N. J. Treat, B. P. Fors, J. W. Kramer, M. Christianson, C.-Y. Chiu, J. Read de Alaniz, C. J. Hawker, *ACS Macro Lett.* **2014**, *3*, 580.
- [33] G. Zhang, I. Y. Song, T. Park, W. Choi, *Green Chem.* **2012**, *14*, 618.
- [34] C.-G. Wang, C. Chen, K. Sakakibara, Y. Tsujii, A. Goto, *Angew. Chem., Int. Ed.* **2018**, *57*, 13504.
- [35] J. Baggerman, M. M. J. Smulders, H. Zuilhof, *Langmuir* **2019**, *35*, 1072.

- [36] H. Vaisocherová-Lísalová, F. Surman, I. Víšová, M. Vala, T. Špringer, M. L. Ermini, H. Šípová, P. Šedivák, M. Houska, T. Riedel, O. Pop-Georgievski, E. Brynda, J. Homola, *Anal. Chem.* **2016**, *88*, 10533.
- [37] H. Lísalová, E. Brynda, M. Houska, I. Víšová, K. Mrkvová, X. C. Song, E. Gedeonová, F. Surman, T. Riedel, O. Pop-Georgievski, J. Homola, *Anal. Chem.* **2017**, *89*, 3524.
- [38] A. T. Nguyen, J. Baggerman, J. M. J. Paulusse, H. Zuilhof, C. J. M. van Rijn, *Langmuir* **2012**, *28*, 604.
- [39] U. Bog, A. de los Santos Pereira, S. L. Mueller, S. Havenridge, V. Parrillo, M. Bruns, A. E. Holmes, C. Rodriguez-Emmenegger, H. Fuchs, M. Hirtz, *ACS Appl. Mater. Interfaces* **2017**, *9*, 12109.
- [40] H. Vaisocherová, V. Ševců, P. Adam, B. Špačková, K. Hegnerová, A. de los Santos Pereira, C. Rodriguez-Emmenegger, T. Riedel, M. Houska, E. Brynda, J. Homola, *Biosens. Bioelectron.* **2014**, *51*, 150.
- [41] H. Kitano, H. Suzuki, K. Matsuura, K. Ohno, *Langmuir* **2010**, *26*, 6767.
- [42] N. Tajima, M. Takai, K. Ishihara, *Anal. Chem.* **2011**, *83*, 1969.
- [43] E. van Andel, S. C. Lange, S. P. Pujari, E. J. Tijhaar, M. M. J. Smulders, H. F. J. Savelkoul, H. Zuilhof, *Langmuir* **2019**, *35*, 1181.
- [44] P. Bisel, L. Al-Momani, M. Müller, *Org. Biomol. Chem.* **2008**, *6*, 2655.
- [45] S. Tugulu, H.-A. Klok, *Biomacromolecules* **2008**, *9*, 906.
- [46] D. Paripovic, H.-A. Klok, *Macromol. Chem. Phys.* **2011**, *212*, 950.
- [47] M. Giesbers, A. T. M. Marcelis, H. Zuilhof, *Langmuir* **2013**, *29*, 4782.
- [48] J. Zhao, F. Gao, S. P. Pujari, H. Zuilhof, A. V. Teplyakov, *Langmuir* **2017**, *33*, 10792.
- [49] Z. Cao, Q. Yu, H. Xue, G. Cheng, S. Jiang, *Angew. Chem., Int. Ed.* **2010**, *49*, 3771.
- [50] A. de los Santos Pereira, T. Riedel, E. Brynda, C. Rodriguez-Emmenegger, *Sens. Actuators, B* **2014**, *202*, 1313.
- [51] A. Laschewsky, A. Rosenhahn, *Langmuir* **2019**, *35*, 1056.
- [52] C.-J. Huang, Y. Li, S. Jiang, *Anal. Chem.* **2012**, *84*, 3440.
- [53] J. W. Weisel, R. I. Litvinov, *Blood* **2013**, *121*, 1712.
- [54] D. Nečas, P. Klapetek, *Open Phys.* **2012**, *10*, 181.
- [55] M. J. Frisch, G. W. Trucks, H. B. Schlegel, G. E. Scuseria, M. A. Robb, J. R. Cheeseman, G. Scalmani, V. Barone, G. A. Petersson, H. Nakatsuji, X. Li, M. Caricato, A. V. Marenich, J. Bloino, B. G. Janesko, R. Gomperts, B. Mennucci, H. P. Hratchian, J. V. Ortiz, A. F. Izmaylov, J. L. Sonnenberg, Williams, F. Ding, F. Lipparini, F. Egidi, J. Goings, B. Peng, A. Petrone, T. Henderson, D. Ranasinghe, V. G. Zakrzewski, J. Gao, N. Rega, G. Zheng, W. Liang, M. Hada, M. Ehara, K. Toyota, R. Fukuda, J. Hasegawa, M. Ishida, T. Nakajima, Y. Honda, O. Kitao, H. Nakai, T. Vreven, K. Throssell, J. A. Montgomery Jr., J. E. Peralta, F. Ogliaro, M. J. Bearpark, J. J. Heyd, E. N. Brothers, K. N. Kudin, V. N. Staroverov, T. A. Keith, R. Kobayashi, J. Normand, K. Raghavachari, A. P. Rendell, J. C. Burant, S. S. Iyengar, J. Tomasi, M. Cossi, J. M. Millam, M. Klene, C. Adamo, R. Cammi, J. W. Ochterski, R. L. Martin, K. Morokuma, O. Farkas, J. B. Foresman, D. J. Fox, *Gaussian 16 Rev. B.01*, Gaussian Inc., Wallingford, CT **2016**.
- [56] E. D. Glendening, A. E. Reed, J. E. Carpenter, F. Weinhold, *NBO (Version 3.1)*, University of Wisconsin, Madison **2003**.